Published in final edited form as:
Magn Reson Med. 2010 May ; 63(5): 1323–1335. doi:10.1002/mrm.22389.

Q-space and Conventional Diffusion Imaging of Axon and Myelin Damage in the Rat Spinal Cord after Axotomy

Jonathan A.D. Farrell[1,2,3], **Jiangyang Zhang**[1], **Melina V. Jones**[4], **Cynthia A. DeBoy**[4], **Paul N. Hoffman**[4,5], **Bennett A. Landman**[6], **Seth A. Smith**[1,2], **Daniel S. Reich**[1,4], **Peter A. Calabresi**[4], and **Peter C.M. van Zijl**[1,2,3]

[1]Russell H. Morgan Department of Radiology and Radiological Science, Johns Hopkins University School of Medicine, Baltimore, Maryland, USA

[2]F.M. Kirby Research Center for Functional Brain Imaging, Kennedy Krieger Institute, Baltimore, Maryland, USA

[3]Department of Biophysics and Biophysical Chemistry, Johns Hopkins University School of Medicine, Baltimore, Maryland, USA

[4]Department of Neurology, Johns Hopkins University School of Medicine, Baltimore, Maryland, USA

[5]Department of Ophthalmology, Johns Hopkins University School of Medicine, Baltimore, Maryland, USA

[6]Department of Biomedical Engineering, Johns Hopkins University, Baltimore, Maryland, USA

Abstract

Parallel and perpendicular diffusion properties of water in the rat spinal cord were investigated 3 and 30 days after dorsal root axotomy, a specific insult resulting in early axonal degeneration followed by later myelin damage in the dorsal column white matter (WM). Results from q-space analysis (i.e. the diffusion probability density function, PDF) obtained with strong diffusion weighting were compared to conventional anisotropy and diffusivity measurements at low b-values, as well as to histology for axon and myelin damage. Q-space contrasts included the height (PZERO), full width at half maximum (FWHM), root mean square displacement (RMSD), and kurtosis excess (KE) of the PDF, which quantifies the deviation from Gaussian diffusion. Following axotomy, a significant increase in perpendicular diffusion (with decreased KE) and decrease in parallel diffusion (with increased KE) were found in lesions relative to uninjured WM. Notably, a significant change in abnormal parallel diffusion was detected from 3 to 30 days with FWHM, but not with conventional diffusivity. Also, directional FWHM and RMSD measurements exhibited different sensitivities to WM damage. When compared to histology, the increase in perpendicular diffusion was not specific to demyelination, whereas combined reduced parallel diffusion and increased perpendicular diffusion was associated with axon damage.

Keywords

q-space imaging; diffusion kurtosis; spinal cord; axotomy; Wallerian degeneration

Corresponding Author: Peter C.M. van Zijl, PhD F.M. Kirby Research Center for Functional Brain Imaging Kennedy Krieger Institute 707 N. Broadway Baltimore, MD 21205 Work: 443-923-9511 Fax: 443-923-9505 pvanzijl@jhu.edu.

INTRODUCTION

Recent Diffusion Tensor Imaging (DTI) studies have suggested that parallel (also termed axial or longitudinal) diffusivity may be sensitive to axonal injury, while perpendicular (also termed radial or transverse) diffusivity may be sensitive to myelin injury (1–4). The prospect that such individual water diffusion properties could potentially report specifically on different types of white matter (WM) injury is exciting. However, the conclusive assignment of changes in diffusion properties to axon and/or myelin damage is not straightforward because axon and myelin damage are often histopathologically linked, and vary in time and space according to the specifics of each disease model. In addition, the biophysics of diffusion is not fully understood and the choice of the diffusion tensor model and the assumptions made for its analysis can have significant ramifications on the quantification of diffusion properties and the potential correlation with WM damage. For instance, DTI approaches commonly work under the assumption of free diffusion (monoexponential diffusion signal attenuation), i.e. corresponding to a Gaussian distribution for the probability density function (PDF). The PDF is the probability that a spin diffuses a given distance from its initial position during the allowed diffusion time. The shape of the PDF contains information about the diffusion environment. A tall, narrow PDF suggests a low diffusion constant, whereas a low, broad PDF suggests a high diffusion constant.

An alternative diffusion weighted MRI (DWI) analysis method is the q-space approach (5–8), which unlike conventional analyses does not assume a pre-defined shape for the PDF. This q-space technique has been applied to study several animal models of spinal cord injury, including myelin development (9,10), WM damage due to crush injury (11), myelin deficiency (12,13), hypertension induced neurodegeneration (14) and experimental allergic encephalomyelitis (EAE) (15). More recently, it has been used to study multiple sclerosis in the human brain (16–18) and spinal cord (19). Q-space contrasts include the height (i.e., the return to zero displacement probability, PZERO), full width at half maximum (FWHM), root mean square displacement (RMSD), and kurtosis excess (KE) (20,21) of the PDF. This later parameter can quantify whether diffusion is free or restricted. A Gaussian PDF has KE = 0, while a PDF that is more peaked and has larger tails than a Gaussian PDF of equal variance has a positive KE. Similar to diffusivity, KE can be reported as the mean value over all orientations ($\overline{KE}$) or alternatively, measured perpendicular ($KE_{\perp}$), or parallel ($KE_{\parallel}$) to the WM fiber orientation. Previous q-space DWI studies have shown that water diffusion in WM is non-Gaussian and have reported the maximum KE over a number of directions in myelin deficient rat brain (22), together with $KE_{\perp}$ in the healthy rat spinal cord (23), mouse spinal cord (24), and human brain (25). Recently, a q-space DWI study of the human brain reported that $\overline{KE}$ is sensitive to WM damage due to multiple sclerosis (18).

The spinal cord, with densely packed myelinated axons oriented in the rostral-caudal direction, is an ideal model system in which to investigate the effects of restricted diffusion and changes in the DWI signal due to WM damage. This *a priori* directional information allows diffusion weighting gradients to be oriented parallel and perpendicular to the WM fiber bundles, which is difficult to achieve in the brain due to its complex fiber architecture. The current study used high resolution *ex vivo* DWI to examine Wallerian degeneration (26) in the rat spinal cord after dorsal root axotomy (27). The time course of WM damage in this model has been well characterized, with dorsal root axotomy resulting in rapid axonal degeneration of the ascending fibers in the dorsal column, followed by delayed demyelination over the course of several weeks, with a distinct lack of an inflammatory response (27–30). The main objective was to compare q-space contrasts to conventional anisotropy and diffusivity measurements and to histology for axon and myelin damage, under the hypothesis that q-space contrasts are more sensitive to WM damage than conventional anisotropy and diffusivity measurements. We also investigated whether changes in diffusion contrasts are specific to axon or myelin damage

identified with histology. We demonstrate that q-space analysis provides a more comprehensive assessment of WM damage and offers several advantages over conventional DWI analysis, including the measurement of the deviation from Gaussian diffusion behavior and sensitivity to the fast and slow diffusion components (under conditions of non-monoexponential decay when using high b-values). This affords improved detection of abnormal diffusion due to WM damage. To our knowledge, this is the first q-space DWI study to report $\overline{KE}$ and $KE_{\parallel}$ in the spinal cord, and the first to report changes in $\overline{KE}$, $KE_{\perp}$, and $KE_{\parallel}$ due to WM damage.

MATERIALS AND METHODS

Theory

The relationship between the measured echo attenuation $E_{tdif}(\mathbf{q})$, the PDF $\bar{P}_s(\mathbf{R}, t_{dif})$ at a given diffusion time t_{dif} and position R, and the loss of phase coherence due to spin displacement is

$$E_{tdif}(\mathbf{q}) = \int \bar{P}_s(\mathbf{R}, t_{dif}) \exp(i2\pi \mathbf{q} \cdot \mathbf{R})\, d\mathbf{R} \quad [1]$$

Where q (a measure of the amount of diffusion weighting) is defined as:

$$\mathbf{q} = \gamma \delta \mathbf{G} / (2\pi) \quad [2]$$

The key principle in q-space analysis is that a Fourier transform (FT) of the signal attenuation with respect to *q* provides the PDF for diffusion:

$$\bar{P}_s(\mathbf{R}, t_{dif}) = FT\{E_{tdif}(\mathbf{q})\} \quad [3]$$

The shape of the PDF can be characterized by the maximum height (i.e., the return to zero displacement probability, PZERO) and full width at half maximum (FWHM) (29). In the specific case of free diffusion (i.e., Gaussian PDF), the diffusion constant *D* and the root mean square displacement (RMSD) for one-dimensional diffusion can be computed from the FWHM (8):

$$RMSD = \frac{FWHM}{2\sqrt{2\ln(2)}} = \sqrt{2Dt_{dif}} \quad [4]$$

Several previous q-space DWI studies have reported the RMSD of the PDF by scaling the FWHM (i.e., RMSD = 0.425 × FWHM) (10,12–16,19,31–33). However, when diffusion is not characterized by a Gaussian PDF (e.g., in the case of non-monoexponential signal attenuation for water diffusion in WM in the central nervous system), the RMSD and FWHM of the PDF may contain unique information and are not related in such a direct way. In this study, the FWHM is computed by linearly interpolating between points on the PDF and the RMSD is computed as:

$$RMSD = \sqrt{\left(\int \bar{P}_s \cdot \mathbf{R}^2 d\mathbf{R}\right)} \quad [5]$$

The kurtosis excess (KE) (20,21) of a distribution offers additional information regarding the shape of the PDF and is defined as:

$$\mathrm{KE}=\left(\mu_4/\mu_2{}^2\right)-3 \quad [6]$$

Where μ_2 (the variance of the PDF) and μ_4 are computed about the mean, μ, according to:

$$\mu_N=\int(\mathrm{R}-\mu)^N\bar{\mathrm{P}}_s(\mathbf{R})\,d\mathbf{R} \quad [7]$$

Animal Preparation

All procedures were approved by the Animal Research Committee of the Johns Hopkins University School of Medicine. Twelve female Lewis rats (160–200g, Charles River Laboratories Inc., Wilmington, MA, USA) were used. Rats were anesthetized with isoflurane and a hemilaminectomy was performed at the L_4 to L_6 vertebral levels to expose the cauda equina on the left side. The left L_2 to L_4 dorsal roots were transected just proximal to the dorsal root ganglion, thereby affecting ascending fibers on the left side of the dorsal column. The wound was closed with wound clips and the animals were allowed to recover. Of the 12 animals, six were permitted to recovery for 3 days, and the remaining six for 30 days. Before *ex vivo* imaging, the rats were deeply anaesthetized and perfused through the heart with cold phosphate buffered saline (PBS) followed by freshly prepared 4% paraformaldehyde. The spinal cords were excised and fixed in 4% paraformaldehyde overnight at 4 °C before transferring to PBS and stored at 4 °C.

Diffusion Weighted MRI

Imaging was performed on an 11.7 Tesla spectrometer equipped with a gradient system capable of a maximum gradient strength of 300 Gauss/cm (Bruker Biospin, Billerica, MA, USA). For the duration of the experiment, spinal cord specimens were kept in a 5 mm NMR tube filled with fomblin (Fomblin Perfluoropolyether, Solvay Solexis, Inc., West Deptford, NJ, USA) to prevent dehydration, and the temperature was maintained at 30 °C via the spectrometer's temperature control system. A 5-mm diameter saddle coil was used as the radio frequency transmitter and signal receiver. Diffusion weighted images (DWIs) of the spinal cord (5 slices centered on L_1, spanning from approximately L_2 to T_{10}) were acquired with a stimulated echo sequence (TR/TE of 1600ms/18.5 ms, acquired resolution of 0.1 × 0.1 × 1.5 mm), with 8 signal averages. DWIs were acquired at 12 q-values from 102 to 1533 cm^{-1} (b_{max}= 74202 s/mm^2) for diffusion weighting perpendicular to the spinal cord (two orientations, G = [1, 0, 0] and [0, 1, 0]), and 8 q-values from 102 to 575 cm^{-1} (b_{max}= 10435 s/mm^2) for diffusion weighting parallel to the spinal cord (G = [0, 0, 1]). The duration (δ = 3ms) and leading edge spacing (Δ = 81 ms) of the diffusion gradients were held constant for all experiments, yielding a diffusion time ($t_{dif} = \Delta - \delta/3$) of 80ms. The b-values and corresponding q-values are shown in table 1.

Data Processing

Data processing was done offline in Matlab (Mathworks, Natick, MA) running on a Sun Fire V880 server (Sun Microsystems, Santa Clara, CA). For signal to noise ratio (SNR) calculations, mean images and difference images were computed from DWIs with diffusion weighting along [1,0,0] and [0,1,0]. The SNR was computed as the mean value in a region of interest (ROI) in the contralateral dorsal column WM in the mean image divided by the standard deviation over the voxels in the same ROI in the difference image. At the level of L_1, the SNR was 30±10 and 7±2 at b-values of 330 and 74202 s/mm^2, respectively (averaged over the 12 rats). An

artificial noise floor was defined as 1.5 times the standard deviation over all voxels in the difference image at b = 74202 s/mm^2. Signal falling below this noise floor in magnitude images was set to zero and these voxels were excluded from analysis.

For the quantification of diffusion perpendicular to the spinal cord, DWIs with diffusion weighting along [1, 0, 0] and [0, 1, 0] were averaged. Conventional analysis was performed by fitting the Stejskal-Tanner equation to the first three points of the signal decay curves at low b-values ($\leq$ 2061 s/mm^2 for both perpendicular and parallel diffusion weighting) where the signal decay appeared mono-exponential. Parallel diffusivity ($D_{\parallel}$), perpendicular diffusivity ($D_{\perp}$), and mean diffusivity (MD) as well as fractional anisotropy (FA) were calculated on a voxel by voxel basis under the assumption of an oriented, cylindrically symmetric tensor.

For q-space analysis, a bi-exponential was fit to the signal decay as a function of b-value. The PDFs for diffusion in the perpendicular and parallel orientations, respectively, were computed from the analytical Fourier transform of each exponential component.

$$\bar{P}_s\left(\mathbf{R}, t_{dif}\right) = \sum_{i=1}^{N} f_i \frac{1}{\sqrt{4\pi D_i t_{dif}}} \exp\left(\frac{-R^2}{4D_i t_{dif}}\right) \quad [8]$$

Where $N = 2$, f_i and D_i are the volume fractions and diffusion constants of each component, and $\sum_{i=1}^{N} f_i = 1$. The KE of a PDF composed of N Gaussian components is given by (34):

$$KE = 3\frac{V(D)}{\left(\bar{D}\right)^2} \quad [9]$$

Where $\bar{D} = \sum_{i=1}^{N} f_i D_i$ and $V(D) \sum_{i=1}^{N} f_i \left(D_i - \bar{D}\right)^2$. Q-space contrast maps were computed on a voxel-by-voxel basis for perpendicular ($PZERO_{\perp}$, $FWHM_{\perp}$, $RMSD_{\perp}$, $KE_{\perp}$) and parallel ($PZERO_{\parallel}$, $FWHM_{\parallel}$, $RMSD_{\parallel}$, $KE_{\parallel}$) diffusion, and the mean kurtosis, $\bar{KE}$, was computed as

$$\bar{KE} = (KE_{\parallel} + 2KE_{\perp})/3 \quad [10]$$

A ROI analysis was performed on a single slice at the L_1 level in each animal. ROIs were delineated on DWIs with diffusion weighting parallel to the spinal cord (b = 2061 s/mm^2) as the lesion was hyperintense on these images. Three ROIs were selected in each animal to include lesioned WM, uninjured contralateral WM, and gray matter (GM), respectively. The ROIs contained approximately 40 voxels. The mean and standard deviation of the ROI-based measurements over the 6 animals in each group are reported.

Histology

Tissues were dissected out of the bone and cut into 11 cross-sectional pieces 5–7mm long. These were pre-embedded together in agar-gelatin (35) and then processed for paraffin embedding by routine procedures. Seven micron thick sections were cut and stained for myelin and axon markers following detailed methods described in (36). Myelin staining was performed with Luxol Fast Blue (LFB), while axon damage was assessed with monoclonal antibody SMI-31 (staining for hyper-phosphorylated neurofilaments indicative of healthy axons),

monoclonal antibody SMI-32 (staining for hypo-phosphorylated neurofilament indicative of damaged axons), and the accumulation of amyloid pre-cursor protein (APP) which indicates an interruption of fast axonal transport. Axon and myelin morphology was assessed by toluidine blue staining (1μm thick cross-sections) following detailed methods described in (36) and examined by light microscopy with a 100× oil-immersion objective lens.

Statistical Analysis

Two-tailed Student's t-Tests, assuming unequal variance, were performed to test the null hypothesis that ROI-based measurements in lesion, and contralateral uninjured WM had equal means (at a significance level of $p = 0.01$). Pair-wise comparisons were made between the lesion at 3 days, the lesion at 30 days, and contralateral uninjured WM. Separate tests were performed for each q-space and conventional DWI contrast. To determine the contrasts that showed the greatest sensitivity to abnormal diffusion, the percent change of each contrast was computed between: (1) the lesion at 3 days and contralateral WM, (2) the lesion at 30 days and contralateral WM, and (3) the lesion at 3 days and lesion at 30 days.

RESULTS

Diffusion Weighted Imaging

The lesion is approximately wedge shaped at the level of L_1 and appears as a hypointensity and hyperintensity in DWIs with perpendicular and parallel diffusion weighting, respectively (Figure 1A, D). The lesion is approximately 0.1 to 0.4 mm wide, and 0.6 mm long and extends from the dorsal surface of the dorsal column to the border with the corticospinal tract at the ventral portion of the dorsal column in agreement with the known course of ascending fibers affected by L_2–L_4 axotomy (37). Signal attenuation curves from representative single voxels in lesion, uninjured contralateral WM, and GM show that for diffusion weighting perpendicular to the long axis of the spinal cord, signal in contralateral WM is preserved even in the high b-value range, whereas signal in the lesion drops off more rapidly with b-value (Figure 1B). The amount of signal attenuation in GM exceeds that found in lesion or healthy WM due to more free diffusion. In the case of diffusion weighting parallel to the long axis of the spinal cord, the signal in contralateral WM falls off rapidly while the signal in the lesion is preserved at higher b-values (Figure 1E). For parallel diffusion, the signal attenuation in healthy GM lies between that found in lesion and healthy WM. Notably, the monoexponential fits from which $D_\perp$ and $D_\parallel$ are calculated describe the data well only at low b-values (< 2061 s/mm^2), while the biexponential function fits the full signal attenuation curve (Figure 1B, E). The PDF for perpendicular diffusion in the lesion is wider and shorter than the PDF in contralateral uninjured WM, and is distinct from the PDF in GM (Figure 1C). For parallel diffusion, the PDF in the lesion is narrower and taller than the PDF in contralateral WM and is distinct from the PDF in GM (Figure 1F).

Figure 2A shows diffusion contrast maps from conventional DWI analysis for two representative animals. At 3 days post axotomy the lesion can be identified as a hyperintensity on the $D_\perp$ map and a hypointensity on the $D_\parallel$, FA, and MD maps with respect to the surrounding WM and uninjured contralateral WM. The lesion is markedly more conspicuous at 30 days post axotomy in the $D_\perp$ and FA maps. In the case of $D_\parallel$, the images at 3 days and 30 days show little difference in lesion conspicuity. The increase of $D_\perp$ and stabilization of $D_\parallel$ between 3 and 30 days results in a pseudo-normalization of MD, with the lesion appearing less conspicuous at 30 days. This is confirmed by the quantitative ROI-based analysis in Figure 2B, showing negligible difference, while measurements of $D_\perp$ and FA were all significantly different ($p < 0.01$) for comparisons of the lesion at 3 days and contralateral WM, the lesion at 30 days and contralateral WM, and the lesion at 3 days and 30 days.

Figure 3A shows q-space contrast maps for diffusion perpendicular to the long axis of the spinal cord. At 3 days post axotomy the lesion can be identified as hyperintense on $FWHM_{\perp}$ and $RMSD_{\perp}$ maps, and hypointense on $PZERO_{\perp}$ and $KE_{\perp}$ maps, with respect to the uninjured contralateral WM. Q-space contrasts for perpendicular diffusion were all abnormal at 3 and 30 days after axotomy compared to uninjured contralateral WM ($p < 0.01$, Figure 3B). The lesion is more conspicuous at 30 days for $RMSD_{\perp}$, $PZERO_{\perp}$ and $KE_{\perp}$ and measurements in lesions at 3 days and 30 days were significantly different ($p < 0.01$) for these three parameters.

Figure 4A shows q-space contrast maps for diffusion parallel to the long axis of the spinal cord. At 3 days post axotomy, the lesion is hypointense on $FWHM_{\parallel}$ and $RMSD_{\parallel}$ maps, and hyperintense on $PZERO_{\parallel}$ and $KE_{\parallel}$ maps. Q-space contrasts for parallel diffusion were all abnormal at 3 and 30 days after axotomy compared to uninjured contralateral WM ($p < 0.01$, Figure 4B). The lesion is more conspicuous at 30 days for $FWHM_{\parallel}$ and $PZERO_{\parallel}$, which is reflected in measurements of $FWHM_{\parallel}$ at 3 days and 30 days being significantly different ($p < 0.01$).

The relative changes for each diffusion parameter both with respect to contralateral normal WM and as a function of time are reported in Table 2. For perpendicular diffusion, $D_{\perp}$, $PZERO_{\perp}$, $FWHM_{\perp}$, $RMSD_{\perp}$, and $KE_{\perp}$ exhibited comparable sensitivity to abnormal diffusion at 3 days, with $D_{\perp}$ exhibiting the largest change, followed by $KE_{\perp}$. $D_{\perp}$ also exhibited the largest abnormality at 30 days (89 % increase), and largest change in contrast for the lesion at 3 and 30 days (66% increase), in both cases followed by $RMSD_{\perp}$. For parallel diffusion, $D_{\parallel}$, $FWHM_{\parallel}$ and $PZERO_{\parallel}$ showed comparable sensitivity to abnormal diffusion at 3 days post axotomy. $KE_{\parallel}$ exhibited the largest lesion contrast (>100%) both at 3 days and 30 days post axotomy. In assessing the lesion contrast change in parallel diffusion from 3 to 30 days, the change in $D_{\parallel}$ was not statistically significant (p=0.4), while $FWHM_{\parallel}$ was (p=0.002), demonstrating an improved detection of abnormal diffusion along the length of the WM fibers with q-space DWI. Mean kurtosis measurements ($\bar{K}E$) were less sensitive than direction-specific KE (i.e., $KE_{\perp}$ and $KE_{\parallel}$) and were not significantly different in lesions at 3 days compared to contralateral WM ($\bar{K}E = 1.56 \pm 0.08$, $\bar{K}E = 1.69 \pm 0.10$, p=0.03), nor in lesions at 30 days compared to contralateral WM ($\bar{K}E = 1.76 \pm 0.10$, $\bar{K}E = 1.46 \pm 0.14$, p=0.02).

Histology of White Matter Damage

Histological assessment of axon and myelin damage in the dorsal column of a control animal, and two separate animals 3 and 30 days after axotomy is shown in Figure 5. At the level of L_1, LFB staining shows negligible change in myelin pallor three days after axotomy, which suggests no demyelination, while LFB shows a visible loss of myelin staining 30 days after axotomy. Staining for axonal markers showed a decrease in SMI-31 and an increase in SMI-32 immunoreactive neurofilament in the lesion three days after axotomy, which suggest significant axon damage. Furthermore, the accumulation of APP three days after axotomy is indicative of an interruption of fast axonal transport. Notably, the decreased detection of SMI-31, increased detection of SMI-32 and accumulation of APP persisted 30 days after axotomy. Figure 6 shows toluidine blue staining of injured and uninjured contralateral WM at 3 and 30 days post-axotomy. At 3 days post-axotomy, the lesion shows the clear presence of several irregularly shaped and enlarged axons. Both healthy and affected axons appear to be surrounded by intact, normal appearing myelin similar to contralateral uninjured WM. At 30 days post-axotomy the effects of WM degeneration are very prominent and the lesion can be clearly distinguished from the uninjured contralateral WM. Notably, several collapsed and degenerating axons show unraveling myelin and have the characteristic appearance of myelin ovoids.

DISCUSSION

Axon and myelin membranes present barriers to water diffusion, and diffusion properties measured perpendicular and parallel to WM fibers can provide information about the microstructural environment. Using conventional DWI analysis, this study found that $D_{\parallel}$ and FA are decreased and $D_{\perp}$ is increased in damaged spinal cord WM after dorsal root axotomy. These findings are in agreement with previous DTI studies of axonal injury, including dorsal root axotomy (36), traumatic injury to the mouse brain (38), spinal cord injury to the mouse spinal cord (39–41), and dorsal column transection in the rat spinal cord (42). DTI studies of EAE (39,43) and WM damage after retinal ischemic injury (3,44,45) have also reported a decrease of $D_{\parallel}$ and an increase in $D_{\perp}$.

This study found a change in several measures of perpendicular diffusion (increased $D_{\perp}$, $FWHM_{\perp}$ and $RMSD_{\perp}$ together with decreased $PZERO_{\perp}$ and $KE_{\perp}$) at 3 days post axotomy without a concomitant loss of LFB staining. This is in agreement with a recent DTI study (36), which included time points spanning from 16 hours to 30 days post axotomy and reported a significant increase in $D_{\perp}$ at 3 days post-axotomy while no significant decrease in LFB staining (quantified with optical-density measurements) was detected at day 3. As confirmation, Zhang *et al*. (36) also reported no change in antibody reactivity to CNPase (2'–3' cyclic nucleotide 3' phosphodiesterase), an alternative stain for myelin, at 3 days post axotomy. The observation of increased perpendicular diffusion early after injury with no noticeable change in LFB staining is in line with findings in previous DTI studies of Wallerian degeneration in the spinal cord. In a model of contusion spinal cord injury, $D_{\perp}$ was increased 7 days post-injury in both LFB-defined spared and demyelinated regions at the site of impact (39). Similarly, in a study of spinal cord injury in mice, $D_{\perp}$ was elevated at 3, 7 and 14 days post-injury in ventral and lateral WM both at and caudal to the site of injury (41). Notably, at 14 days post-injury LFB demonstrated demyelination at the injury impact site (with elevated $D_{\perp}$), however LFB staining caudal to the injury site was qualitatively similar to controls (in contrast to the elevated $D_{\perp}$ in this region) (41). One factor to consider, that may account for elevated perpendicular diffusion at 3 and 30 days post axotomy, is that irregularities in the myelin sheath (as shown in Figure 6) have been noted early after the onset of granular degeneration of the axon cytoskeleton and include: irregular folding and splitting of the myelin lamellae to form concentric rings around the degenerating axon, and contraction of the sheath concurrent with collapse and fragmentation of the axon (27,29,46). These morphological changes may not result in changes in LFB staining. Taken together, our findings of an elevated $D_{\perp}$ at 3 days post-axotomy suggest that perpendicular diffusion may be sensitive to a host of factors (e.g. changes in membrane permeability, axon and myelin morphology, and intra- and extra-cellular water populations) in addition to the prominent demyelination that occurs in late stages following dorsal root axotomy. In the future, studies that combine DTI, q-space imaging, and quantitative histology at multiple closely spaced time points may further clarify the causal relationship between myelin damage, myelin loss, and the increase in diffusion perpendicular to WM tracts.

The reduction in parallel diffusion (reflected in decreased $D_{\parallel}$, $FWHM_{\parallel}$, and $RMSD_{\parallel}$, together with increased $PZERO_{\parallel}$ and $KE_{\parallel}$) in lesions at 3 and 30 days post axotomy is likely due to additional barriers to parallel diffusion. These barriers may be imposed by axonal beading (formation of bulges along the length of the axon (47)), the fragmentation of the axon into short sections (myelin ovoids) encompassed by myelin and the accumulation and slow removal of axon and myelin debris (which can persist up to 90 days) in the dorsal root axotomy model (27–30). This interpretation is consistent with the increased staining for SMI-32 and APP (Figure 5), which indicates degeneration of the cytoskeleton and breakdown of fast-axon transport, respectively, and the abnormal axon and myelin morphology consistent with the formation of myelin ovoids (Figure 6). Previous DTI studies have also noted a decrease of

$D_{\parallel}$ with increased APP and SMI-32 staining after axon injury (36,38,43,45). The emerging relationship between the breakdown of axon transport, accumulation of proteins (such as APP and degraded cytoskeleton components) and axonal organelles at localized sites, axonal bead formation, and Wallerian degeneration in several central nervous system disorders is covered in a recent compressive review (28). In related work, Monte-Carlo simulations of water diffusion showed that axon damage (modeled as periodic bulges along the length of impermeable cylinders) can cause a reduction in $D_{\parallel}$ and FA, and an increase in $D_{\perp}$ and $KE_{\parallel}$ (48,49). This suggests that axonal beading may play a prominent role in reducing parallel diffusion. In the future, more comprehensive and realistic models of tissue damage could be developed by incorporating both intra- and extra-axonal water, molecular exchange, relaxation, and biologically relevant geometries (49). Additionally, the interpretation of changes in parallel diffusion may benefit significantly from the recent elucidation of the spatiotemporal evolution of axon pathology by fluorescent microscopy studies (30,50).

Our study found a decrease of $D_{\parallel}$ at 3 days, which was maintained at 30 days post injury. This is in agreement with previous DTI studies of Wallerian degeneration that have reported that $D_{\parallel}$ is decreased after axon injury, including transient retinal ischemia in mice (3,44,45), dorsal root axotomy in the rat spinal cord (36), and spinal cord transection (42). While the initial decrease in $D_{\parallel}$ may be sensitive to axonal degeneration, a consistent level of reduced $D_{\parallel}$ during an extended period of axon and myelin debris removal is somewhat surprising. Notably, the temporal evolution of $D_{\parallel}$ in animal models which exhibit a breakdown of the blood-brain, or blood-spinal cord barrier after injury is quite different, owing perhaps to the effects of edema and macrophage infiltration which accelerate debris clearance. Compared to our findings of a maintained level of decreased $D_{\parallel}$, an initial decrease in $D_{\parallel}$ followed by a pseudo-normalization that remained below, or reached control levels has been reported after traumatic spinal cord injury (41) and traumatic brain injury (38), respectively. A decrease in $D_{\parallel}$, however, is not ubiquitous across different models of WM damage and changes in parallel diffusion are likely closely related to the specific pathology and the time after injury at which diffusion is measured for each disease process or injury model. Evidence of this is that a DTI study of myelin deficient rat spinal cords (51) has reported that both $D_{\perp}$ and $D_{\parallel}$ are increased relative to normal WM. Notably, an increase in $D_{\parallel}$ can also occur during tissue recovery as noted by Sun *et al.* (4), who reported a transient decrease of $D_{\parallel}$ in the corpus callosum of mice during cuprizone administration, followed by a normalization of $D_{\parallel}$ which persisted during the recovery phase. The need to reconcile these differences, find contrasts that are more sensitive to tissue damage, and understand how changes in diffusion properties correlate with microstructural changes motivates the performance of DWI experiments over a wide range of b-values and the utilization of analysis techniques, such as q-space analysis, that can quantify non-Gaussian diffusion behavior.

In this study, a prominent departure from mono-exponential signal attenuation was observed at high b-values ($b > 2000$ s/mm^2) for perpendicular diffusion in both lesioned WM and uninjured WM (Figure 1B). The non-Gaussian diffusion in damaged WM 30 days post axotomy is notable and suggests that many barriers to perpendicular diffusion persist despite the effects of demyelination. This makes sense in view of the fact that myelin is not the sole contributor to restricted diffusion (52) and the vacuolation and astrogliosis (53) that occurs during the later stages of Wallerian degeneration may provide sufficient barriers to diffusion. Furthermore, non-Gaussian diffusion was also observed for parallel diffusion in GM, lesioned WM, and uninjured WM (Figure 1E). In principle, the signal attenuation for water diffusion along the length of healthy axons is expected to be mono-exponential as a function of the b-value due to the lack of structural barriers to water displacement in this orientation (52). However, the structural heterogeneity of WM fiber bundles over the size of an MRI voxel may provide sufficient barriers to parallel diffusion to result in non-Gaussian diffusion in healthy WM. This finding is consistent with previous reports of $KE_{\parallel} > 0$ in healthy WM (Table 3).

In agreement with previous q-space DWI studies of rat spinal cord injury (11–14), this study found a significant increase in perpendicular diffusion in lesions compared to contralateral WM. Parallel q-space diffusion properties have been less well explored, possibly due to SNR considerations when using very high b-values. However, the findings that parallel diffusion is decreased (decreased $FWHM_{\parallel}$, $RMSD_{\parallel}$, increased $PZERO_{\parallel}$) agrees with a study of crush injury in the rat spinal cord (11) and EAE in the swine spinal cord (15). Our values for $\bar{KE}$ in healthy GM (0.39 ± 0.08), together with $\bar{KE}$ (1.7 ± 0.1), $KE_{\perp}$ (2.3 ± 0.2), and $KE_{\parallel}$ (0.42 ± 0.07) in healthy WM are in good agreement with previous q-space studies of the human brain *in vivo* (18,25), together with diffusion kurtosis imaging (DKI) studies of the human brain *in vivo* (18,25,34,54), the rat brain *ex vivo* (55,56), and the rat spinal cord *ex vivo* (57) (Table 3). DKI (34,54) is methodologically distinct from q-space DWI and can also be used to quantify the deviation from Gaussian diffusion, though is limited to intermediate b-values (< 2500 s/mm^2). Notably, however, two recent q-space DWI studies in the rat (23) and mouse spinal cords (24) have reported significantly larger $KE_{\perp}$ values in spinal cord WM. This difference could, in part, be due to acquisition parameters and methodological considerations which are discussed in more detail in the technical considerations section of the current work.

Our findings of a significant decrease of $KE_{\perp}$ and increase of $KE_{\parallel}$ in response to WM damage in the dorsal root axotomy model can probably be explained by the loss of axon and/or myelin barriers to diffusion in the perpendicular direction and the introduction of additional barriers to diffusion in the parallel direction, respectively. One important finding of this q-space DWI study is the demonstration that directional KE measurements (i.e., $KE_{\perp}$ and $KE_{\parallel}$) are more sensitive to abnormal diffusion in damaged WM than $\bar{KE}$ measurements, in line with results from a recent DKI study of EAE in the rat spinal cord (57). Though no significant change in $\bar{KE}$ was measured in the current study, a decrease of $\bar{KE}$ has been reported for multiple sclerosis lesions in the human brain (18).

One of the specific goals of this study was to compare the sensitivity of conventional DWI contrasts (computed at low b-values) and q-space contrasts to abnormal diffusion due to WM damage at the early and later stages of Wallerian degeneration (Table 2). An important finding of the current study was that, in the case of parallel diffusion, the only contrast to exhibit a statistically significant difference from 3 to 30 days was $FWHM_{\parallel}$ (decreased by 24%, $p = 0.002$). By comparison, $D_{\parallel}$ decreased at 3 days and remained unchanged at 30 days, in agreement with the findings from a recent DTI study (36). This suggests that high b-value q-space DWI may be more sensitive to the evolving morphological changes that occur during the time course of Wallerian degeneration and their effect on diffusion parallel to the WM fiber orientation. The decrease of $FWHM_{\parallel}$ suggests a more restricted diffusion environment at 30 days compared to 3 days, which may be due to the formation of degenerating tissue characterized by vacuolation and astrogliosis (53). In the future, q-space and DTI experiments that include later time points (perhaps up to 90 days in the case of dorsal root axotomy (27, 29)) may further elucidate the sensitivity of parallel diffusion properties to the clearance of myelin and axon debris. Additionally, while the PZERO, FWHM and RMSD can be expressed in terms of each other for a Gaussian PDF, this is not the case, in general, for non-Gaussian PDFs. In this study, PZERO, FWHM and RMSD exhibited significantly different sensitivities to WM damage in the perpendicular and parallel orientations. This is well illustrated by the fact that a large increase of $RMSD_{\perp}$ was measured from 3 to 30 days post axotomy, while no significant change in $FWHM_{\perp}$ was noted. Interestingly, $FWHM_{\parallel}$ was sensitive to the change in abnormal diffusion from 3 to 30 days, while no significant change in $RMSD_{\parallel}$ was noted. This observation may be due to different sensitivities of FWHM and RMSD to the fast and slow diffusion components. It is therefore a recommendation of this study that both RMSD and FWHM measurements are reported in q-space DWI studies as the information provided by these contrasts could be different.

Technical Considerations

Q-space analysis offers two key advantages compared to conventional DWI analysis: sensitivity to both the fast and slow diffusion components, and the ability to quantify non-Gaussian diffusion. Though this new information comes with the cost of additional scan time and SNR constraints at high b-values, which may prohibit some *in vivo* applications, it is encouraging to note that q-space DWI of multiple sclerosis is feasible in the human brain (16–18) and spinal cord (19). An additional benefit of q-space analysis is that measurements of restricted diffusion can be combined with tissue models to extract morphological properties such as axon diameter, together with intra and extra-cellular water fractions (23,24,32). Though careful histological validation is needed, this approach may have the potential to elucidate tissue microstructure at the sub-voxel level.

A necessary consideration is that acquisition parameters (which are also relevant for diffusion metrics obtained with DTI) can affect the size and shape of the PDF. Important factors include the duration of the diffusion weighting gradients (δ), the prescribed diffusion time (t_{dif}), and the spatial resolution of the PDF (Δx) which is determined by:

$$\Delta_x = 1/(N\Delta q) = 1/q_{\max} \quad [11]$$

where N is the number of q-values acquired in steps of Δq up to q_{max}. Simulation-based (58, 59) and experimental studies of restricted diffusion in microcapillary tubes (60,61), together with imaging studies of the rat sciatic nerve (16) and spinal cord (62) have shown that, at a fixed q_{max}, long diffusion gradient pulses (i.e. violation of the short gradient pulse (SGP) criteria, $\delta << \Delta$) produce PDFs that are narrower (and correspondingly taller) than would be expected based on the size of the confining geometry. Despite this limitation, the magnitude of the bias is small (FWHM decreased by a factor of two when δ was increased from 4.5 to 72ms in the sciatic nerve (16), and decreased by 10% when δ was increased from 2 to 20ms in a study of the rat spinal cord (62)). The time that molecules have to explore their local environment also has a strong effect on measured diffusion properties and longer diffusion times have recently been shown to enhance the contrast between GM and WM on q-space contrast maps of perpendicular diffusion (62). Based on the results presented by Bar-Shir *et al*. (61) who investigated the effect of δ and Δ/δ, the parameters used in the current study (δ =3ms, Δ =80ms) are sufficient to ensure accurate displacement measurements and good contrast between GM and WM.

Despite this improved understanding, it is not clear how violation of the SGP criteria will affect KE measurements. One possibility is that the overemphasis of the slow diffusion component may produce elevated KE values that suggest a larger degree of non-Gaussian diffusion. A separate issue is that KE is expected to be particularly sensitive to the overall shape of the PDF, and may be prone to bias when the calculated PDF fails to adequately represent the true diffusion process. This is relevant when Δx is too large and the signal attenuation fails to decay to approximately 1 to 4% of the original value. In this instance the PDF contains few points and erroneously high KE values can be obtained, as shown by a recent simulation study (63). While linear interpolation of PDFs with large Δx may provide reasonable displacement values, this approach may not be suitable for the accurate quantification of KE. To combat this, the signal attenuation can be zero-filled or extrapolated prior to the FT in order to decrease Δx. However, zero-filling can introduce ringing artifacts into the PDF which may further complicate the calculation of KE. To address this, Latt *et al*. (64) have suggested the use of a cut-off value whereby the outer portions of the PDF (<1% of PZERO) are set to zero to prevent erroneously high and noisy KE values. Notably, the current study assumed a bi-exponential fit to the signal attenuation and computed KE from the analytical Fourier transform of the fit components to avoid the effects of Δx and ringing artifacts. Overall, the inter-study comparison

of KE values and interpretation of KE in healthy and diseased neural tissue would both benefit from a detailed assessment of the effect of acquisition parameters and signal processing procedures. Research on this topic, building on the preliminary findings presented in (63), is currently under way.

CONCLUSION

Q-space analysis provides a more comprehensive assessment of WM damage and offers several key advantages over conventional DWI analysis including the measurement of the kurtosis excess of diffusion and the quantification of both the fast and slow diffusion components. While the initial increase in perpendicular diffusion was not specific to demyelination, the decrease in parallel diffusion may be a specific marker for initial axon damage. Finally, for non-Gaussian behavior, the relationship between RMSD and FWHM is not straightforward and it is recommended that these PDF-based contrasts are reported separately.

Acknowledgments

This publication was made possible by Grant Number P41 RR015241 from the National Center for Research Resources (NCRR), a component of the National Institutes of Health (NIH), NIH AG20012, NIH NS052309, and NIH NS059529 together with grants from the National MS Society CA 1029-A-2, TR-3760-A-3; and the Nancy Davis Center without Walls. Its contents are solely the responsibility of the authors and do not necessarily represent the official view of NCRR or NIH.

Grant Support: NIH/NCRR P41RR15241; National MS Society CA 1029-A-2, TR-3760-A-3; NIH AG20012; NIH NS052309; NIH NS059529; Nancy Davis Center without Walls.

REFERENCES

1. Song SK, Sun SW, Ramsbottom MJ, Chang C, Russell J, Cross AH. Dysmyelination revealed through MRI as increased radial (but unchanged axial) diffusion of water. NeuroImage 2002;17(3):1429–1436. [PubMed: 12414282]
2. Song SK, Yoshino J, Le TQ, Lin SJ, Sun SW, Cross AH, Armstrong RC. Demyelination increases radial diffusivity in corpus callosum of mouse brain. NeuroImage 2005;26(1):132–140. [PubMed: 15862213]
3. Sun SW, Liang HF, Cross AH, Song SK. Evolving Wallerian degeneration after transient retinal ischemia in mice characterized by diffusion tensor imaging. NeuroImage 2008;40(1):1–10. [PubMed: 18187343]
4. Sun SW, Liang HF, Trinkaus K, Cross AH, Armstrong RC, Song SK. Noninvasive detection of cuprizone induced axonal damage and demyelination in the mouse corpus callosum. Magn Reson Med 2006;55(2):302–308. [PubMed: 16408263]
5. Callaghan P, Codd S, Seymour J. Spatial Coherence Phenomena Arising from Translational Spin Motion in Gradient Spin Echo Experiments Concepts. Magn Reson 1999;11:181–202.
6. Callaghan P, Coy A, MacGowan D, Packer K, Zelaya F. Diffraction-like effects in NMR diffusion studies of fluid in porous solids. Nature 1991;351:467–469.
7. Cohen Y, Assaf Y. High b-value q-space analyzed diffusion-weighted MRS and MRI in neuronal tissues - a technical review. NMR in biomedicine 2002;15(7–8):516–542. [PubMed: 12489099]
8. Cory DG, Garroway AN. Measurement of translational displacement probabilities by NMR: an indicator of compartmentation. Magn Reson Med 1990;14(3):435–444. [PubMed: 2355827]
9. Assaf Y, Cohen Y. Assignment of the water slow-diffusing component in the central nervous system using q-space diffusion MRS: implications for fiber tract imaging. Magn Reson Med 2000;43(2):191–199. [PubMed: 10680682]
10. Assaf Y, Mayk A, Cohen Y. Displacement imaging of spinal cord using q-space diffusion-weighted MRI. Magn Reson Med 2000;44(5):713–722. [PubMed: 11064406]

11. Nossin-Manor R, Duvdevani R, Cohen Y. q-Space high b value diffusion MRI of hemi-crush in rat spinal cord: evidence for spontaneous regeneration. Magnetic resonance imaging 2002;20(3):231–241. [PubMed: 12117605]
12. Biton IE, Duncan ID, Cohen Y. High b-value q-space diffusion MRI in myelin-deficient rat spinal cords. Magnetic resonance imaging 2006;24(2):161–166. [PubMed: 16455404]
13. Biton IE, Duncan ID, Cohen Y. q-Space diffusion of myelin-deficient spinal cords. Magn Reson Med 2007;58(5):993–1000. [PubMed: 17969109]
14. Assaf Y, Mayk A, Eliash S, Speiser Z, Cohen Y. Hypertension and neuronal degeneration in excised rat spinal cord studied by high-b value q-space diffusion magnetic resonance imaging. Experimental neurology 2003;184(2):726–736. [PubMed: 14769364]
15. Biton IE, Mayk A, Kidron D, Assaf Y, Cohen Y. Improved detectability of experimental allergic encephalomyelitis in excised swine spinal cords by high b-value q-space DWI. Experimental neurology 2005;195(2):437–446. [PubMed: 16098966]
16. Assaf Y, Ben-Bashat D, Chapman J, Peled S, Biton IE, Kafri M, Segev Y, Hendler T, Korczyn AD, Graif M, Cohen Y. High b-value q-space analyzed diffusion-weighted MRI: application to multiple sclerosis. Magn Reson Med 2002;47(1):115–126. [PubMed: 11754450]
17. Assaf Y, Chapman J, Ben-Bashat D, Hendler T, Segev Y, Korczyn AD, Graif M, Cohen Y. White matter changes in multiple sclerosis: correlation of q-space diffusion MRI and 1H MRS. Magnetic resonance imaging 2005;23(6):703–710. [PubMed: 16198825]
18. Latt J, Nilsson M, Wirestam R, Johansson E, Larsson EM, Stahlberg F, Brockstedt S. In vivo visualization of displacement-distribution-derived parameters in q-space imaging. Magnetic resonance imaging 2008;26(1):77–87. [PubMed: 17582719]
19. Farrell JAD, Smith SA, Gordon-Lipkin EM, Reich DS, Calabresi PA, van Zijl PCM. High b-value q-space diffusion-weighted MRI of the human cervical spinal cord in vivo: feasibility and application to multiple sclerosis. Magn Reson Med 2008;59(5):1079–1089. [PubMed: 18429023]
20. Balanda KP, MacGillivray HL. Kurtosis: a critical review. The American Statistician 1988;42(2): 111–119.
21. DeCarlo LT. On the meaning and use of kurtosis. Psychological Methods 1997;2(3):292–307.
22. Bar-Shir A, Duncan ID, Cohen Y. QSI and DTI of excised brains of the myelin-deficient rat. NeuroImage 2009;48(1):109–116. [PubMed: 19539038]
23. Chin CL, Wehrli FW, Fan Y, Hwang SN, Schwartz ED, Nissanov J, Hackney DB. Assessment of axonal fiber tract architecture in excised rat spinal cord by localized NMR q-space imaging: simulations and experimental studies. Magn Reson Med 2004;52(4):733–740. [PubMed: 15389948]
24. Ong HH, Wright AC, Wehrli SL, Souza A, Schwartz ED, Hwang SN, Wehrli FW. Indirect measurement of regional axon diameter in excised mouse spinal cord with q-space imaging: simulation and experimental studies. NeuroImage 2008;40(4):1619–1632. [PubMed: 18342541]
25. Chabert, S.; Meca, CC.; Le Bihan, D. Relevance of the information about the diffusion distribution in vivo given by kurtosis in q-space imaging. Proceedings of the 12th Annual Scientific Meeting of the International Society for Magnetic Resonance in Medicine; Kyoto, Japan. 2004.
26. Waller A. experiments on the sections of glossopharyngeal and hypoglossal nerves of the frog and observations of the alterations produced thereby in the structure of their primitive fibers. Phil Trans R Soc Lond 1850;140:423–429.
27. George R, Griffin JW. The proximo-distal spread of axonal degeneration in the dorsal columns of the rat. Journal of neurocytology 1994;23(11):657–667. [PubMed: 7861182]
28. Coleman M. Axon degeneration mechanisms: commonality amid diversity. Nature reviews 2005;6 (11):889–898.
29. George R, Griffin JW. Delayed macrophage responses and myelin clearance during Wallerian degeneration in the central nervous system: the dorsal radiculotomy model. Experimental neurology 1994;129(2):225–236. [PubMed: 7957737]
30. Kerschensteiner M, Schwab ME, Lichtman JW, Misgeld T. In vivo imaging of axonal degeneration and regeneration in the injured spinal cord. Nature medicine 2005;11(5):572–577.
31. Assaf Y, Mayzel-Oreg O, Gigi A, Ben-Bashat D, Mordohovitch M, Verchovsky R, Reider G II, Hendler T, Graif M, Cohen Y, Korczyn AD. High b value q-space-analyzed diffusion MRI in vascular dementia: a preliminary study. Journal of the neurological sciences 2002;203–204:235–239.

32. Bar-Shir A, Cohen Y. High b-value q-space diffusion MRS of nerves: structural information and comparison with histological evidence. NMR in biomedicine 2008;21(2):165–174. [PubMed: 17492659]
33. Biton IE, Mayk A, Assaf Y, Cohen Y. Structural changes in glutamate cell swelling followed by multiparametric q-space diffusion MR of excised rat spinal cord. Magnetic resonance imaging 2004;22(5):661–672. [PubMed: 15172060]
34. Jensen JH, Helpern JA, Ramani A, Lu H, Kaczynski K. Diffusional kurtosis imaging: the quantification of non-gaussian water diffusion by means of magnetic resonance imaging. Magn Reson Med 2005;53(6):1432–1440. [PubMed: 15906300]
35. Jones MV, Calabresi PA. Agar-gelatin for embedding tissues prior to paraffin processing. Biotechniques 2007;42(5):569–570. [PubMed: 17515193]
36. Zhang J, Jones M, DeBoy CA, Reich DS, Farrell JA, Hoffman PN, Griffin JW, Sheikh KA, Miller MI, Mori S, Calabresi PA. Diffusion tensor magnetic resonance imaging of Wallerian degeneration in rat spinal cord after dorsal root axotomy. J Neurosci 2009;29(10):3160–3171. [PubMed: 19279253]
37. Smith KJ, Bennett BJ. Topographic and quantitative description of rat dorsal column fibres arising from the lumbar dorsal roots. Journal of anatomy 1987;153:203–215. [PubMed: 3429320]
38. Mac Donald CL, Dikranian K, Bayly P, Holtzman D, Brody D. Diffusion tensor imaging reliably detects experimental traumatic axonal injury and indicates approximate time of injury. J Neurosci 2007;27(44):11869–11876. [PubMed: 17978027]
39. Budde MD, Kim JH, Liang HF, Schmidt RE, Russell JH, Cross AH, Song SK. Toward accurate diagnosis of white matter pathology using diffusion tensor imaging. Magn Reson Med 2007;57(4): 688–695. [PubMed: 17390365]
40. Ford JC, Hackney DB, Alsop DC, Jara H, Joseph PM, Hand CM, Black P. MRI characterization of diffusion coefficients in a rat spinal cord injury model. Magn Reson Med 1994;31(5):488–494. [PubMed: 8015401]
41. Kim JH, Loy DN, Liang HF, Trinkaus K, Schmidt RE, Song SK. Noninvasive diffusion tensor imaging of evolving white matter pathology in a mouse model of acute spinal cord injury. Magn Reson Med 2007;58(2):253–260. [PubMed: 17654597]
42. Kozlowski P, Raj D, Liu J, Lam C, Yung AC, Tetzlaff W. Characterizing white matter damage in rat spinal cord with quantitative MRI and histology. Journal of neurotrauma 2008;25(6):653–676. [PubMed: 18578635]
43. Kim JH, Budde MD, Liang HF, Klein RS, Russell JH, Cross AH, Song SK. Detecting axon damage in spinal cord from a mouse model of multiple sclerosis. Neurobiology of disease 2006;21(3):626–632. [PubMed: 16298135]
44. Song SK, Sun SW, Ju WK, Lin SJ, Cross AH, Neufeld AH. Diffusion tensor imaging detects and differentiates axon and myelin degeneration in mouse optic nerve after retinal ischemia. NeuroImage 2003;20(3):1714–1722. [PubMed: 14642481]
45. Sun SW, Liang HF, Le TQ, Armstrong RC, Cross AH, Song SK. Differential sensitivity of in vivo and ex vivo diffusion tensor imaging to evolving optic nerve injury in mice with retinal ischemia. NeuroImage 2006;32(3):1195–1204. [PubMed: 16797189]
46. Friede RL, Martinez AJ. Analysis of axon-sheath relations during early Wallerian degeneration. Brain research 1970;19(2):199–212. [PubMed: 4315394]
47. Ochs S, Pourmand R, Jersild RA Jr. Friedman RN. The origin and nature of beading: a reversible transformation of the shape of nerve fibers. Progress in neurobiology 1997;52(5):391–426. [PubMed: 9304699]
48. Farrell, JAD.; Landman, BA.; Zhang, J.; Smith, SA.; Reich, DS.; Calabresi, PA.; Van Zijl, PCM. The effect of axonal “beading” on water diffusion properties: a monte carlo simulation of axonal degeneration and its effects on DTI contrasts. Proceedings of: The 17th annual scientific meeting of the International Society for Magnetic Resonance in Medicine; Honolulu, HI. 2009.
49. Landman BA, Farrell JA, Smith SA, Reich DS, Calabresi PA, van Zijl PC. Complex geometric models of diffusion and relaxation in healthy and damaged white matter. NMR in biomedicine. 2009 DOI: 10.1002/nbm.1437.

50. Beirowski B, Berek L, Adalbert R, Wagner D, Grumme DS, Addicks K, Ribchester RR, Coleman MP. Quantitative and qualitative analysis of Wallerian degeneration using restricted axonal labelling in YFP-H mice. Journal of neuroscience methods 2004;134(1):23–35. [PubMed: 15102500]
51. Gulani V, Webb AG, Duncan ID, Lauterbur PC. Apparent diffusion tensor measurements in myelin-deficient rat spinal cords. Magn Reson Med 2001;45(2):191–195. [PubMed: 11180424]
52. Beaulieu C. The basis of anisotropic water diffusion in the nervous system - a technical review. NMR in biomedicine 2002;15(7–8):435–455. [PubMed: 12489094]
53. Buss A, Schwab ME. Sequential loss of myelin proteins during Wallerian degeneration in the rat spinal cord. Glia 2003;42(4):424–432. [PubMed: 12730963]
54. Lu H, Jensen JH, Ramani A, Helpern JA. Three-dimensional characterization of non-gaussian water diffusion in humans using diffusion kurtosis imaging. NMR in biomedicine 2006;19(2):236–247. [PubMed: 16521095]
55. Cheung MM, Hui ES, Chan KC, Helpern JA, Qi L, Wu EX. Does diffusion kurtosis imaging lead to better neural tissue characterization? A rodent brain maturation study. NeuroImage 2009;45(2):386–392. [PubMed: 19150655]
56. Hui ES, Cheung MM, Qi L, Wu EX. Towards better MR characterization of neural tissues using directional diffusion kurtosis analysis. NeuroImage 2008;42(1):122–134. [PubMed: 18524628]
57. Cheung, MM.; Hui, ES.; Wu, W.; Wu, EX. Comparison of directional diffusion kurtoses and diffusivities in EAE-induced spinal cord. Proceedings of the 16th Annual Scientific Meeting of the International Society for Magnetic Resonance in Medicine; Toronto, Canada. 2008.
58. Coy A, Callaghan PT. Pulsed gradient spin echo nuclear magnetic resonance for molecules diffusing between partially reflecting rectangular barriers. J Chem Phys 1994;101:4599–4609.
59. Mitra PP, Halperin BI. Effects of finite gradient-pulse widths in pulsed-field-gradient diffusion measurements. J Magn Reson A 1995;113(1):94–101.
60. Avram L, Assaf Y, Cohen Y. The effect of rotational angle and experimental parameters on the diffraction patterns and micro-structural information obtained from q-space diffusion NMR: implication for diffusion in white matter fibers. J Magn Reson 2004;169(1):30–38. [PubMed: 15183354]
61. Bar-Shir A, Avram L, Ozarslan E, Basser PJ, Cohen Y. The effect of the diffusion time and pulse gradient duration ratio on the diffraction pattern and the structural information estimated from q-space diffusion MR: experiments and simulations. J Magn Reson 2008;194(2):230–236. [PubMed: 18667345]
62. Nossin-Manor R, Duvdevani R, Cohen Y. Effect of experimental parameters on high b-value q-space MR images of excised rat spinal cord. Magn Reson Med 2005;54(1):96–104. [PubMed: 15968658]
63. Farrell, JAD. Q-space Diffusion Imaging of Axon and Myelin Damage in the Human and Rat Spinal Cord. Johns Hopkins University School of Medicine; Baltimore, Maryland: 2009. p. 266
64. Latt J, Nilsson M, Malmborg C, Rosquist H, Wirestam R, Stahlberg F, Topgaard D, Brockstedt S. Accuracy of q-space related parameters in MRI: simulations and phantom measurements. IEEE transactions on medical imaging 2007;26(11):1437–1447. [PubMed: 18041259]

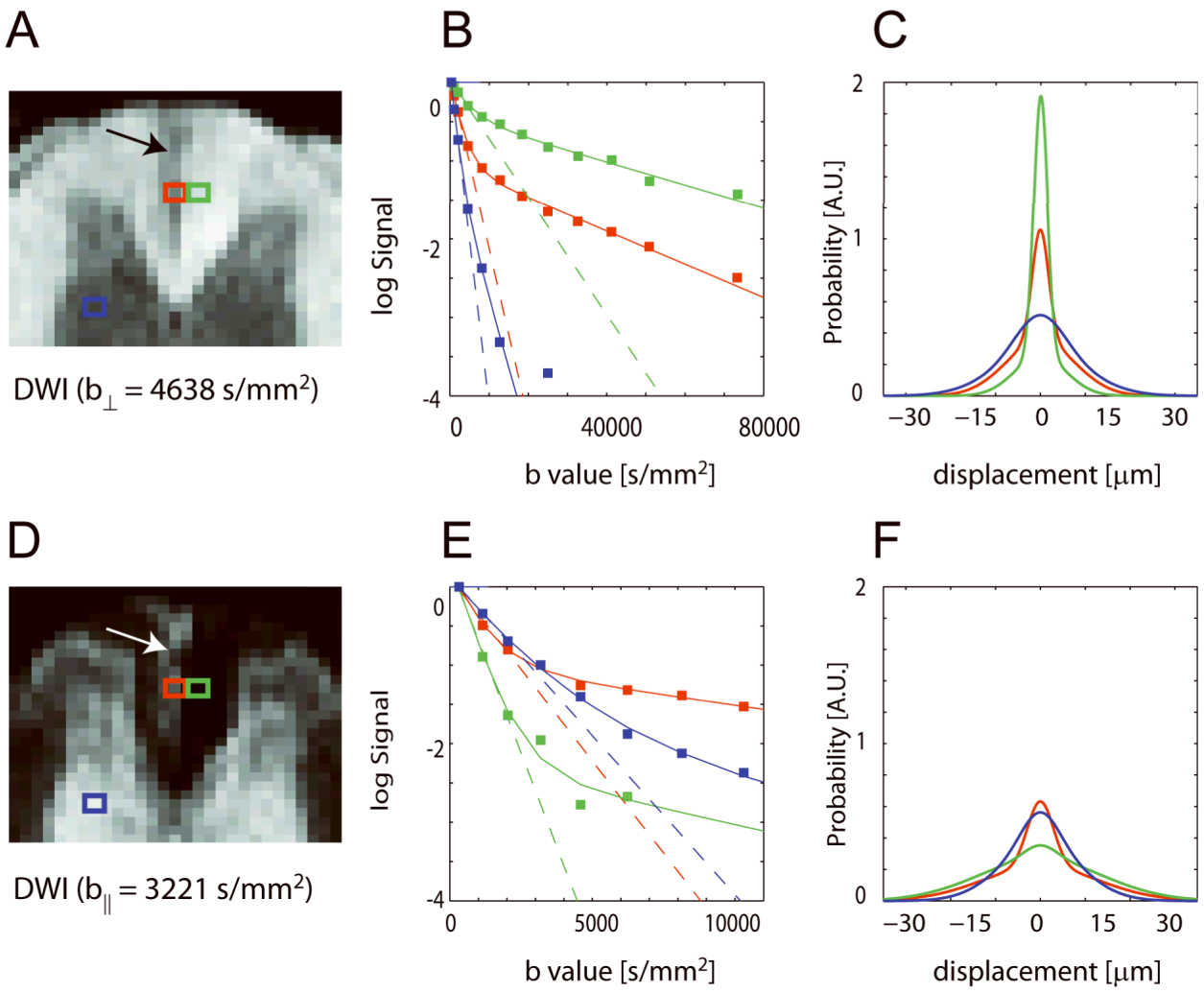

Figure 1.

Diffusion weighted images of the dorsal column at the level of L_1, signal attenuation curves, and computed PDFs for diffusion perpendicular (⊥) (A–C) and parallel (∥) (D–F) to the long axis of the rat spinal cord 30 days after axotomy. The location of the lesion in the left dorsal column is indicated (arrows). Results for single voxels in lesion (red), uninjured contralateral WM (green), and GM (blue) are shown. The monoexponential fit to the signal attenuation at low b-values and the bi-exponential fit over all b-values are indicated by dotted and solid lines, respectively.

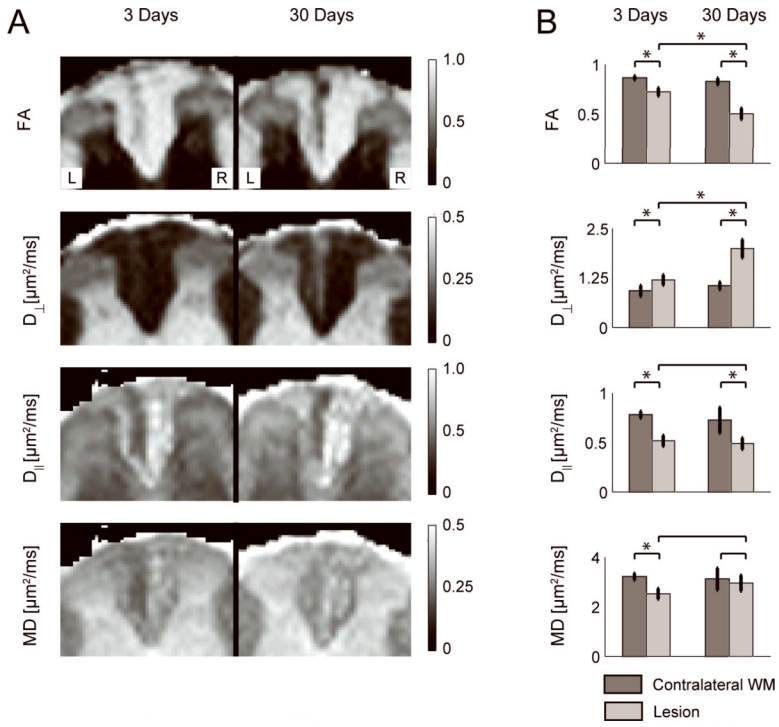

Figure 2.

A) Fractional anisotropy (FA), perpendicular diffusivity ($D_{\perp}$), parallel diffusivity ($D_{\parallel}$), and mean diffusivity (MD) maps for an animal at 3 days (left image) and another animal at 30 days (right image) post-axotomy. **B)** ROI analysis of the conventional DWI contrasts in the contralateral WM (dark bars) and lesion (light bars) over the 6 animals in each group. * denotes significant difference ($p < 0.01$).

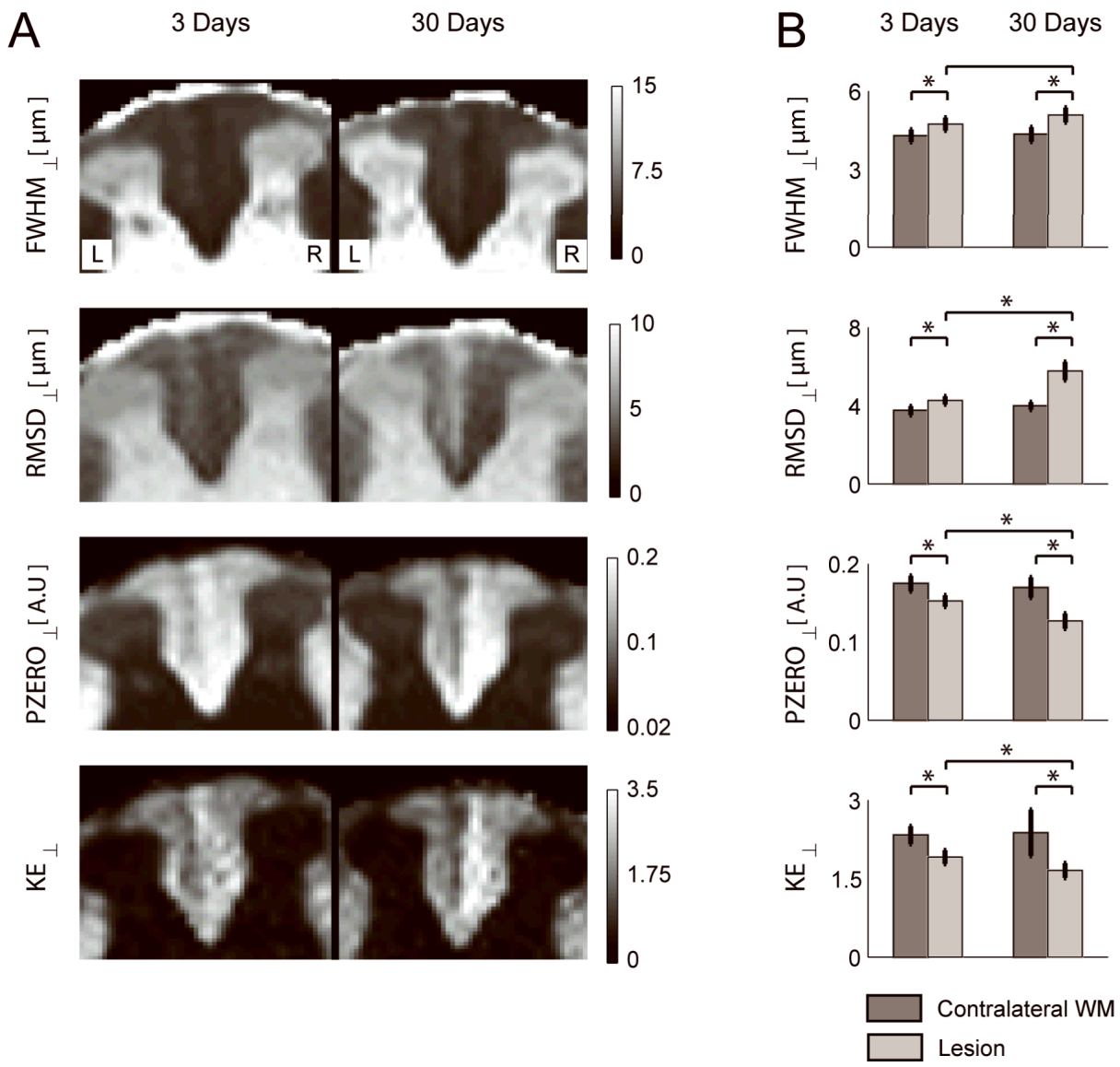

Figure 3.

A) Maps of the full width at half maximum ($FWHM_{\perp}$), root mean square displacement ($RMSD_{\perp}$, height ($PZERO_{\perp}$), and kurtosis excess ($KE_{\perp}$) of the PDF for perpendicular diffusion for an animal at 3 days (left image) and another animal at 30 days (right image) post-axotomy. **B)** ROI analysis of the q-space contrasts in the contralateral WM (dark bars) and lesion (light bars) over the 6 animals in each group. * denotes significant difference ($p < 0.01$).

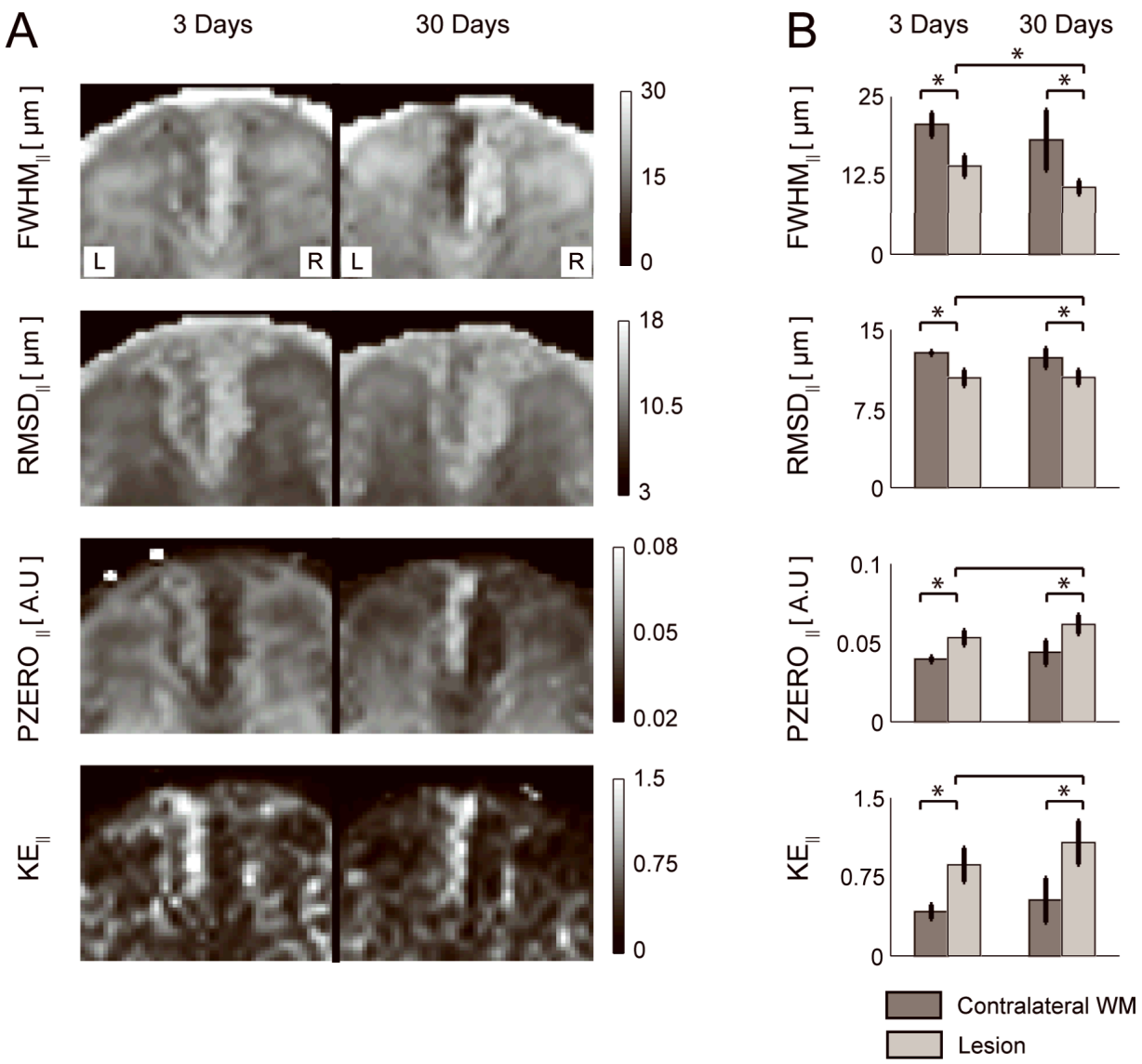

Figure 4.

A) Maps of the full width at half maximum ($FWHM_{\parallel}$), root mean square displacement ($RMSD_{\parallel}$), height ($PZERO_{\parallel}$), and kurtosis excess ($KE_{\parallel}$) of the PDF for parallel diffusion in an animal at 3 days (left image) and another animal at 30 days (right image) post-axotomy. **B)** ROI analysis of the q-space contrasts in the contralateral WM (dark bars) and lesion (light bars) over the 6 animals in each group. * denotes significant difference ($p < 0.01$).

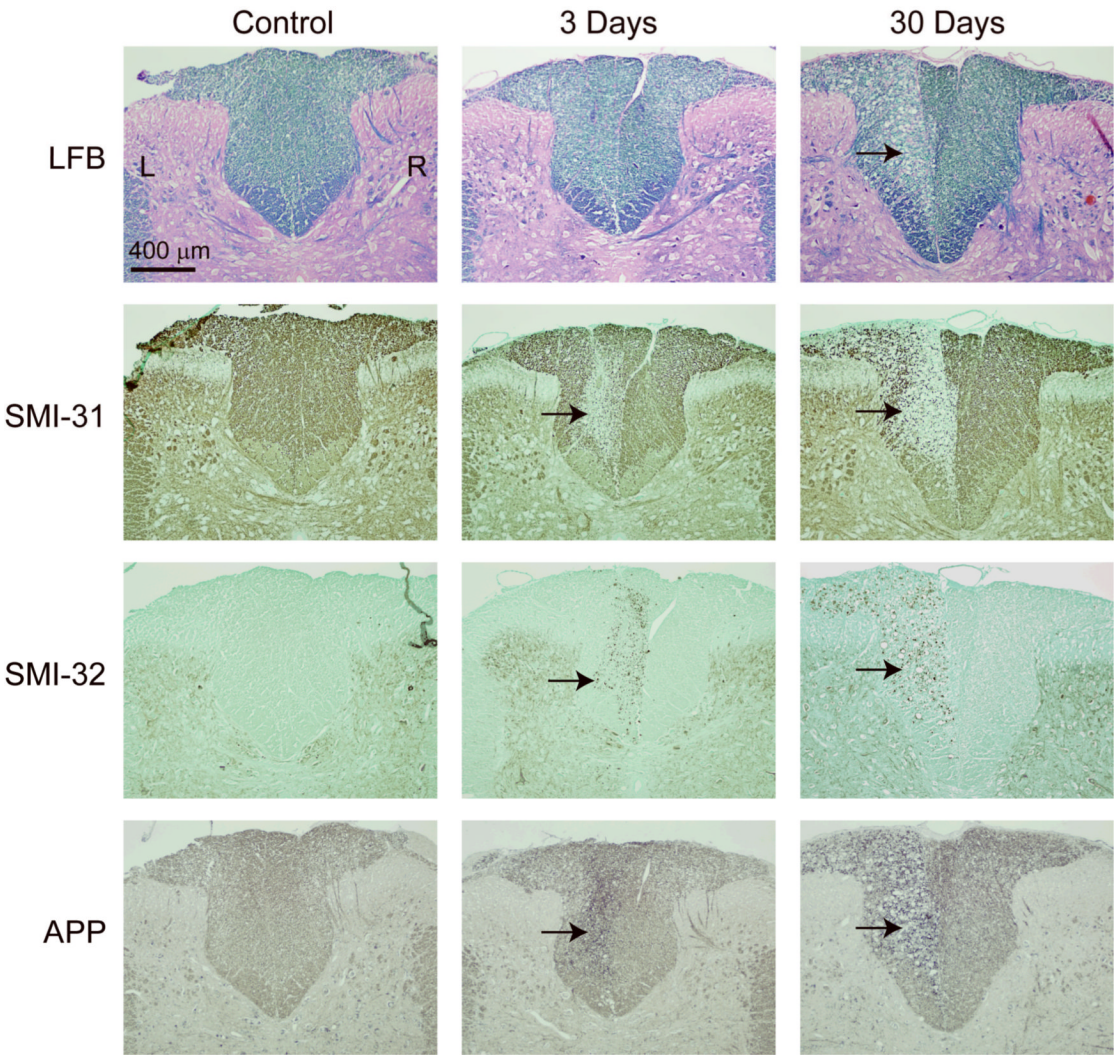

Figure 5.
Histological images of the dorsal column WM of the rat spinal cord. Images are shown for a control animal, and animals 3 and 30 days after axotomy. Stains include luxol fast blue (LFB) for myelin, SMI-31 for phosphorylated neurofilament, SMI-32 for hypo-phosphorylated neurofilament, and APP for amyloid pre-cursor protein. The location of the lesion in the left dorsal column is indicated by black arrows.

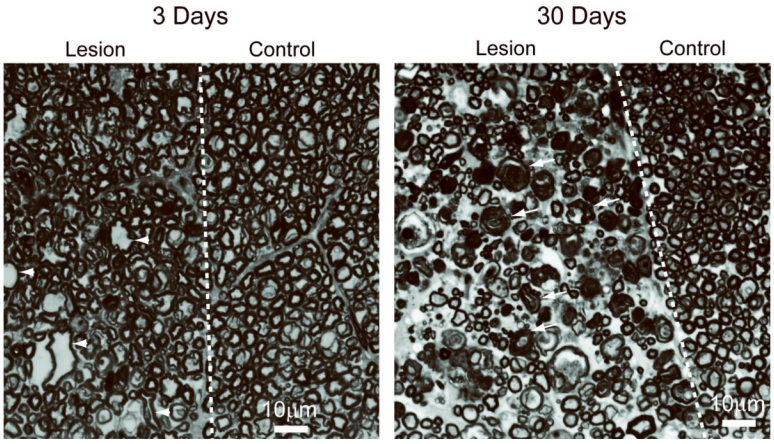

Figure 6.
Grayscale images of toluidine blue staining of the dorsal column WM of the rat spinal cord at 3 and 30 days after axotomy. Examples of irregularly shaped and enlarged axons (arrowheads), and collapsed, degenerating axons surrounded by unraveling myelin (arrows) are indicated. The scale bar indicates 10 μm.

Table 1

b-values and corresponding q-values for images with diffusion weighting perpendicular (⊥) and parallel (∥) the long axis of the spinal cord at t_{dif} = 80ms.

Perpendicular (⊥)		**Parallel (∥)**	
b-value [s/mm^2]	**q-value [1/cm]**	**b-value [s/mm^2]**	**q-value [1/cm]**
330	102	330	102
1010	179	1159	192
2061	255	2061	255
4638	383	3221	319
8245	511	4638	383
12882	639	6312	447
18550	766	8245	511
25249	894	10435	575
32979	1022		
41739	1150		
51529	1277		
74202	1533		

Table 2

The relative change of diffusion contrasts between lesions at 3 days, 30 days, and uninjured contralateral white matter.

Contrast	Lesion at 3 Days Vs. Uninjured WM		Lesion at 30 Days Vs. Uninjured WM		Lesion at 30 Days vs. Lesion at 3 Days	
	Change (%)	p-value	Change (%)	p-value	Change (%)	p-value
FA	−16 ± 5	* < 0.0001	−39 ± 8	* < 0.0001	−31 ± 10	* < 0.0001
$D_{\perp}$	30 ± 21	* 0.005	89 ± 26	* < 0.0001	66 ± 23	* < 0.0001
$D_{\parallel}$	−34 ± 9	* < 0.0001	−33 ± 21	* 0.002	−5 ± 16	0.4
MD	−22 ± 8	* < 0.0001	−5 ± 18	0.5	17 ± 15	0.02
$FWHM_{\perp}$	10 ± 8	* 0.009	17 ± 9	* 0.001	7 ± 8	0.05
$RMSD_{\perp}$	14 ± 9	* 0.002	45 ± 13	* < 0.0001	35 ± 12	* < 0.0001
$PZERO_{\perp}$	−13 ± 7	* 0.001	−25 ± 10	* < 0.0001	−17 ± 8	* 0.0004
$KE_{\perp}$	−18 ± 9	* 0.0007	−30 ± 20	* 0.004	−13 ± 10	* 0.0091
$FWHM_{\parallel}$	−32 ± 13	* < 0.0001	−41 ± 29	* 0.004	−24 ± 14	* 0.002
$RMSD_{\parallel}$	−18 ± 6	* < 0.0001	−15 ± 9	* 0.003	0 ± 10	0.9
$PZERO_{\parallel}$	35 ± 13	* < 0.0001	41 ± 23	* 0.001	16 ± 14	0.02
$KE_{\parallel}$	106 ± 45	* < 0.0001	103 ± 69	* 0.001	24 ± 31	0.08
$\overline{KE}$	−8 ± 8	0.03	−17 ± 16	0.02	−6 ± 10	0.2

Positive (negative) values denote an increase (decrease) in the diffusion measure relative to the uninjured contralateral WM (columns 1 and 2) or relative to the lesion 3 days after axotomy (column 3).

*denotes significant difference ($p < 0.01$) for the ROI analysis presented in Figures 2B, 3B and 4B.

Table 3

Comparison of mean ($\overline{KE}$) and directional kurtosis excess ($KE_{\perp}$ and $KE_{\parallel}$) values from DKI and q-space DWI studies of water diffusion in healthy gray matter and white matter.

Kurtosis Measure		Organism/Organ	Tissue Type	Study	Reference
Gray Matter					
$\overline{KE}$	0.30 ± 0.05	Human Brain	GM	Q-space	(25)
	0.51 ± 0.12	″	put	Q-space	(18)
	0.38 ± 0.05	″	put	DKI	(18)
	0.82 ± 0.03	″	Cortical GM	DKI	(34)
	0.74 ± 0.03	″	GM	DKI	(54)
	0.87 ± 0.03	Rat Brain	cpt	DKI	(56)
	0.93 ± 0.03	″	Ex vivo, cpt	DKI	(56)
	0.39 ± 0.08	Rat Spinal Cord	Ex vivo, GM	Q-space	This study
White Matter					
$\overline{KE}$	0.26 ± 0.04	Human Brain	cc	Q-space	(25)
	0.81 ± 0.12	″	deep WM	Q-space	(18)
	0.84 ± 0.03	″	deep WM	DKI	(18)
	0.65 ± 0.17	″	cc	Q-space	(18)
	0.72 ± 0.07	″	cc	DKI	(18)
	1.41 ± 0.11	″	frontal WM	DKI	(34)
	1.09 ± 0.01	″	Brain	DKI	(54)
	1.02 ± 0.03	Rat Brain	cc	DKI	(56)
	1.60 ± 0.10	″	Ex vivo, cc	DKI	(56)
	$1.1 \pm 0.1^{+}$	Rat Spinal Cord	Ex vivo, WM	DKI	(57)
	1.7 ± 0.1	″	Ex vivo, gracilis tract	Q-space	This study
$KE_{\perp}$	0.59 ± 0.15	Human Brain	Optic radiation	Q-space	(25)
	1.55 ± 0.10	Rat Brain	cc	DKI	(56)
	1.94 ± 0.15	″	Ex vivo, cc	DKI	(56)
	$1.5 \pm 0.1^{+}$	″	cc	DKI	(55)

Kurtosis Measure		Organism/Organ	Tissue Type	Study	Reference
	11.4 ± 0.2	″	cc	DKI	(22)
	17 ± 1 and 55 ± 5*	Mouse Spinal Cord	Ex vivo, gracilis tract	Q-space	(24)
	9.51**	Rat Spinal Cord	Ex vivo, gracilis tract	Q-space	(23)
	2.1 ± 0.2+	″	Ex vivo, WM	DKI	(57)
	2.3 ± 0.2	″	Ex vivo, gracilis tract	Q-space	This study
$KE_{\parallel}$	0.29 ± 0.09	Human Brain	Optic radiation	Q-space	(25)
	0.74 ± 0.03	Rat Brain	cc	DKI	(56)
	1.30 ± 0.06	″	Ex vivo, cc	DKI	(56)
	0.75 ± 0.1+	″	cc	DKI	(55)
	0.6 ± 0.1+	Rat Spinal Cord	Ex vivo, WM	DKI	(57)
	0.42 ± 0.07	″	Ex vivo, gracilis tract	Q-space	This study

Putamen (put), caudate and putatmen (cpt), corpus callosum (cc). KE values for cortical gray matter in the human brain (18), (34), and thalamus (54) are not listed. For this study, the average value across 6 rats (3 days post axotomy) is reported for ROIs in uninjured dorsal column WM and GM.

*estimated from graph for cases satisfying narrow gradient pulse with and without truncation.

**error estimate not provided.

+Estimated from graph.